Polyhedron 73 (2014) 1–11

Contents lists available at ScienceDirect

Polyhedron

journal homepage: www.elsevier.com/locate/poly

Ruthenium complexes with Schiff base ligands containing benz(othiazole/imidazole) moieties: Structural, electron spin resonance and electrochemistry studies

Irvin N. Booysen *, Abimbola Adebisi, Orde Q. Munro, Bheki Xulu

School of Chemistry and Physics, University of Kwazulu-Natal, Private Bag X01, Scottsville 3209, Pietermaritzburg, South Africa

ARTICLE INFO

Article history:
Received 2 November 2013
Accepted 5 February 2014
Available online 15 February 2014

Keywords:
Ruthenium(II/III)
Schiff bases
Benz(imidazole/othiazole)
Electron spin resonance
Structural
Electrochemistry

ABSTRACT

Novel ruthenium(II/III) complexes of Schiff bases containing benzimidazole (bz) or benzothiazole (bs) moieties were isolated: the diamagnetic ruthenium complex, *cis*-[$Ru^{II}Cl_2$(bzpy)$(PPh_3)_2$] (**1**) was formed from the 1:1 M reaction between *N*-((pyridine-2-*yl*)methylene)-1*H*-benzimidazole (bzpy) and metal precursor, *trans*-[$RuCl_2(PPh_3)_3$]. The same metal precursor, when reacted with the benzimidazole-derived Schiff bases [*N*-(2-hydroxybenzylidene)-benzothiazole (Hbsp) and *N*-(2-hydroxybenzylidene)-benzimidazole (Hbzp)], afforded the paramagnetic ruthenium(III) complexes [RuCl$(bsp)_2(PPh_3)$] (**2**) and *trans*-[RuCl$(bzp)(PPh_3)_2$] (**3**), respectively. These metal complexes were characterized *via* IR, mass and UV–Vis spectroscopy, elemental analysis, single crystal XRD analysis as well as conductivity measurements. Their redox properties were probed by voltammetry and accompanying UV–Vis spectroelectrochemistry experiments. Structural features of complex **1** were further investigated by multinuclear (^{1}H and ^{31}P) NMR spectroscopy. The presence of the paramagnetic metal centres of **2** and **3** were confirmed by X-band ESR spectroscopy.

1. Introduction

The discovery of NAMI A, *trans*-[$RuCl_4$(DMSO)(Im)](ImH) {ImH = imidazole} as a potential metallopharmaceutical for metastatic cancer, has led to a renewed interest into the medicinal inorganic chemistry of ruthenium [1–7]. In particular, ruthenium complexes with N-donor heterocyclic ligands have been widely investigated due to their diverse biological activities [8–12]. From a coordination chemistry perspective, this class of ligand systems afford ruthenuim complexes with unique coordination environments, owing to the diverse donor atom combinations and resulting metal chelation [13–16]. In addition, they can have variable stereo-electronic properties arising from their ability to form neutral or multivalent anionic N-donor chelators which inevitably allows for stabilization of the metal centre both in low and high oxidation states [8–20].

In this account, we report the reactions of *trans*-[$RuCl_2(PPh_3)_3$] with the Schiff bases derived from heterocyclic moieties [*N*-((pyridine-2-*yl*)methylene)-1*H*-benzimidazole (bzpy), *N*-(2-hydroxybenzylidene)-benzothiazole (Hbsp) and *N*-(2-hydroxybenzylidene)-benzimidazole (Hbzp] to afford the ruthenium complexes: *cis*-[$Ru^{II}Cl_2$(bzpy)$(PPh_3)_2$] (**1**), [RuCl$(bsp)_2(PPh_3)$] (**2**) and *trans*-[RuCl$(bzp)(PPh_3)_2$] (**3**), respectively. Despite the similar skeletal structures of the ligands, ruthenium complexes with diverse structural features were isolated. This diversity is also manifest in their redox and electronic properties.

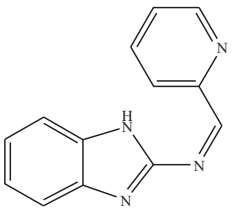

bzpy

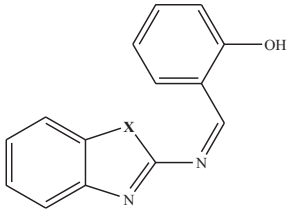

X = S (Hbsp)
N (Hbzp)

2. Experimental

2.1. Materials and methods

Trans-[$RuCl_2(PPh_3)_3$], 2-aminobenzothiazole (2-NH_2-bs), 2-aminobenzimidazole (2-NH_2-bz), salicylaldehyde, 2-pyridylaldehyde and electrochemical analysis grade tetrabutylammonium hexa-

* Corresponding author. Tel.: +27 797378626; fax: +27 332605009.
E-mail address: Booyseni@ukzn.ac.za (I.N. Booysen).

http://dx.doi.org/10.1016/j.poly.2014.02.009
0277-5387/

fluorophosphate were obtained from Sigma Aldrich. All solvents were obtained from Merck SA. Reagent grade toluene was dried over sodium wire while the other solvents and chemicals were used without any further purification. Ultrapure water was produced from an Elga Purelab Ultra system. The Schiff base ligands derived from salicylaldehyde were synthesized from modified experimental procedures as previously reported [21,22]. For Hbsp and Hbzp, the respective (1:1 M ratio) condensation reactions between 2-NH_2-bs and 2-NH_2-bz with salicylaldehyde were done in dry refluxing toluene, under a nitrogen atmosphere and in the presence of catalytic amounts of piperidine.

The infrared spectra were recorded on a Perkin-Elmer Spectrum 100 in the 4000–650 cm^{-1} range. The ^{1}H NMR spectra were obtained using Bruker Avance 400 MHz and 500 MHz spectrometers, respectively. The X-band EPR spectrum was obtained from a Bruker EMX Ultra X spectrometer. All NMR spectra were recorded in DMSO-d_6. UV–Vis spectra were recorded using a Perkin Elmer Lambda 25. The extinction coefficients (ε) are given in dm^3 mol^{-1} cm^{-1}. Mass spectral analysis of the complexes was done both in positive and negative modes *via* the direct injection of the respective samples into the Water Micromass LCT Premier instrument equipped with a Time-of-Flight (TOF) Mass spectrometer analyzer and an Electronspray Ionization (ESI) source. Melting points were determined using a Stuart SMP3 melting point apparatus. The conductivity measurements were determined at 295 K on a Radiometer R21M127 CDM 230 conductivity and pH meter. Elemental composition of the complexes was determined using ThermoScientific Flash 2000 CHNS/O Analyser.

Cyclic voltammetry measurements were done using an Autolab potentiostat equipped with a three electrode system: a glassy carbon working electrode (GCWE), a pseudo Ag|AgCl reference electrode and an auxiliary Pt counter electrode. The Autolab Nova 1.7 software was utilized for the operation of the potentiostat and data analysis. The ruthenium metal complexes were made up in 2 mM solutions in DCM along with tetrabutylammonium hexafluorophosphate (0.1 M) as a supporting electrolyte. Between each measurement, the GCWE electrode surface was polished with a slurry of ultrapure water and alumina on a Buehler felt pad followed by rinsing with excess ultrapure water and ultra-sonication in absolute ethanol. Spectroelectrochemical data were attained using a room temperature Specac optically transparent thin-layer electrochemical (OTTLE) cell purchased from the University of Reading which was connected to the Autolab potentiostat.

2.2. N-((pyridine-2-yl)methylene)-1H-benzimidazole (Bzpy)

A mixture of 2-aminobenzimidazole (0.500 g; 3.76 mmol) and 2-pyridinecarboxaldehyde (0.400 g; 3.76 mmol) was heated until reflux for 3 h in methanol (20 cm^3), along with 1 cm^3 of piperidine. The resulting yellow solution was allowed to cool to room temperature and concentrated under reduced pressure. Afterwards dry toluene (40 cm^3) was added to the solution and heated to reflux for 6 h with a Dean and Stark apparatus. A yellow precipitate was filtered and washed with cold anhydrous toluene. Yield = 75%, m.p. 236–238 °C. IR (ν_{max}/cm^{-1}): ν(N–H) 3051 (w), ν(C=N)$_{Schiff\ base}$ 1612 (s), ν(C=N)$_{Heterocyclic}$ 1587 (s); ^{1}H NMR (295 K/ppm/d^6-DMSO): 12.82 (br, s, 1H, N3*H*), 9.36 (s, 1H, *H6*), 8.80 (d, 1H, *J* = 7.61 Hz, *H1*), 8.03 (t, 1H, *J* = 8.03 Hz, *H3*), 7.67–7.46 (m, 3H, *H2*, *H10*, *H11*), 7.24–7.17 (m, 2H, *H9*, *H12*); ^{13}C NMR (295 K/ppm/d^6-DMSO): 165.50, 153.67, 150.71, 137.82, 127.01, 122.81, 122.16. UV–Vis (DCM, (λ_{max} (ε, M^{-1} cm^{-1}))): 255 (sh, 2300); 284 (1980); 360 (2480).

2.3. Cis-Cl, trans-P [$Ru^{II}Cl_2$(bzpy)(PPh_3)$_2$] (**1**)

A mixture of bzpy (0.0231 g; 0.104 mmol) and *trans*-[$RuCl_2$(PPh_3)$_3$] (0.100 g; 0.104 mmol) in dry toluene (20 cm^3) was heated to reflux under a nitrogen atmosphere for 6 h. The volume of the resultant dark brown solution was reduced to half and then *n*-hexane was added dropwise to induce precipitation. In turn, the dark brown precipitate was recrystallized *via* slow diffusion in a dichloromethane and *n*-hexane [1:1 (*v*:*v*)] solution which resulted in the formation of dark brown XRD quality parallelograms. Yield = 63%, m.p. >350 °C. IR (ν_{max}/cm^{-1}): ν(N–H) 3067 (w), ν(C=N)$_{Heterocyclic}$ 1635 (s), ν(C=N)$_{Schiff\ base}$ 1606 (s), ν(Ru-[PPh_3]$_2$) 696 (s); ^{1}H NMR (295 K/ppm/d^6-DMSO): 8.97 (s, 1H, N3*H*), 8.47 (s, 1H, *H6*), 7.66–7.60 (m, 4H, *H1*, *H2*, *H3*, *H4*), 7.58–7.54 (m, 4H, *H9*, *H10*, *H11*, *H12*), 7.43–7.38 (m, 15H, PPh_3), 7.27–7.22 (m, 15H, PPh_3); ^{31}P NMR (295 K/ppm/d^6-DMSO): 25.57. UV–Vis (DCM, (λ_{max} (ε, M^{-1} cm^{-1}))): 301 (12 800); 358 (sh, 10 100); 410 (sh, 7620); 435 (sh, 5480); 576 (3220). Conductivity (DCM, 10^{-3} M): 15.51 ohm^{-1} cm^{-2} mol^{-1}. *Anal.* Calc. for $C_{49}H_{40}Cl_2N_4P_2Ru$: C, 64.05; H, 4.39; N, 6.10. Found: C, 63.97; H, 4.01; N, 6.32%. TOF-MS (*m*/*z*): Calcd: 918.11 [M]; Found: 848.164 [M−2Cl].

2.4. [RuCl(bsp)$_2$(PPh_3)] (**2**)

A two molar ratio of Hbsp (0.0530 g; 0.208 mmol) with respect to the metal precursor, *trans*-[$RuCl_2$(PPh_3)$_3$] (0.100 g; 0.104 mmol) were reacted together in refluxing toluene (20 cm^3) for 6 h. After the addition of 10 cm^3 acetonitrile to the mother liquor and from the slow evaporation of the resultant mixture, dark brown crystals were attained for X-ray analysis. Yield = 66%, m.p. = 236–238 °C. IR (ν_{max}/cm^{-1}): ν(C=N)$_{Schiff\ base}$ 1588 (m), ν(C=N)$_{Heterocyclic}$ 1531 (m), ν(C=C) 1435 (s), ν(Ru-PPh_3) 693 (s). UV–Vis (DCM, (λ_{max} (ε, M^{-1} cm^{-1}))): 279 (sh, 16 200); 328 (sh, 10 900); 524 (1800); 705 (800). Conductivity (DCM, 10^{-3} M): 19.38 ohm^{-1} cm^{-2} mol^{-1}. *Anal.* Calc. for $C_{46}H_{33}ClN_4O_2PRuS_2$: C, 61.02; H, 3.67; N, 6.19. Found: C, 60.56; H, 4.01; N, 6.39%. TOF-MS (*m*/*z*): Calcd: 905.05 [M]; Found: 905.049 [M].

2.5. Trans-[RuCl(bzp)(PPh_3)$_2$] (**3**)

The title compound was formed from the 1:1 M ratio reaction of Hbzp (0.0247 g; 0.104 mmol) and *trans*-[$RuCl_2$(PPh_3)$_3$] (0.100 g; 0.104 mmol) in (20 cm^3) toluene (after 6 h of refluxing). From the slow evaporation of the mother liquor, brown needle-like crystals suitable for X-ray analysis were obtained after 3 days. Yield = 71%, m.p. = 256–258 °C. IR (ν_{max}/cm^{-1}): ν(N–H) 3062 (w), ν(C=N)$_{Schiff\ base}$ 1679 (m), ν(C=N)$_{Heterocyclic}$ 1589 (m), ν(C=C) 1433 (m), ν[Ru-(PPh_3)$_2$] 691. UV–Vis (DCM, (λ_{max} (ε (10^3), M^{-1} cm^{-1}))): 270 (sh, 17 900); 320 (sh, 10 900); 385 (sh, 7030); 544 (sh, 1790); 692 (860). Conductivity (DCM, 10^{-3} M): 28.74 ohm^{-1} cm^{-2} mol^{-1}. *Anal.* Calc. for $C_{57}H_{47}P_2ClRuON_3$: C, 69.26; H, 4.79; N, 4.25. Found: C, 68.87; H, 4.54; N, 4.75%. TOF-MS (*m*/*z*): Calcd: 896.13 [M for 3]; Found: 895.142 [M−H].

2.6. X-ray diffraction

The X-ray data for all the metal complexes were recorded on a Bruker Apex Duo equipped with an Oxford Instruments Cryojet operating at 100(2) K and an Incoatec microsource operating at 30 W power. Crystal and structure refinement data are given in Table 1. Selected bond lengths and angles are given in Tables 2–4. In all three cases the data were collected with Mo Kα (λ = 0.71 073 Å) radiation at a crystal-to-detector distance of 50 mm. The following conditions were used for the Bruker data collection: omega and phi scans with exposures taken at 30 W X-ray power and 0.50° frame widths using APEX2 [23]. The data were reduced with the programme SAINT [49] using outlier rejection, scan speed scaling, as well as standard Lorentz and polarization correction factors. A SADABS [24] semi-empirical multi-scan absorption correction was applied to the data [25]. Direct meth-

Table 1
Crystal data and structure refinement data.

	1	**2**	**3**·C_7H_8
Chemical formula	$C_{49}H_{40}Cl_2N_4P_2Ru$	$C_{46}H_{33}ClN_4O_2PRuS_2$	$C_{57}H_{47}P_2ClRuON_3$
Formula weight	918.76	905.4	988.44
T (K)	100(2)	100(2)	100(2)
Crystal system	triclinic	monoclinic	triclinic
Space group	$P\bar{1}$	P_12_1/n	$P\bar{1}$
Unit cell dimensions			
a (Å)	12.2629(6)	12.6611(5)	11.9756(10)
b (Å)	13.4789(6)	23.4989(8)	12.7076(11)
c (Å)	14.8725(7)	13.1178(5)	15.1112(13)
α (°)	104.012(2)	90.00	97.670(4)
β (°)	101.332(2)	91.807(2)	91.750(4)
γ (°)	114.289(2)	90.00	90.061(4)
Crystal size (mm)	0.35 × 0.10 × 0.08	0.17 × 0.12 × 0.01	0.20 × 0.15 × 0.08
V (Å^3)	2048.54(17)	3900.89(4)	2278.0(3)
Z	2	4	2
D_{calc} (Mg/m^3)	1.490	1.54	1.441
Absorption coefficient (mm^{-1})	0.63	0.665	0.519
F(000)	940.00	1843.7	1018.0
θ (°)	1.5; 30.53	1.7; 29.3	1.6; 27.08
Index ranges	$-17 \leqslant h \leqslant 17$, $-19 \leqslant k < 19$, $-21 \leqslant l \leqslant 21$	$-17 \leqslant h \leqslant 17$, $-27 \leqslant k < 32$, $-18 \leqslant l \leqslant 18$	$-15 \leqslant h \leqslant 15$, $-15 \leqslant k < 16$, $-18 \leqslant l \leqslant 17$
Reflections measured	46486	42006	21774
Observed reflections [$I > 2\sigma(I)$]	12336	8949	8911
Independent reflections	11489	10638	7569
Data/restraints/parameters	11489/0/582	10638/0/509	7569/0/587
Goodness of fit (GOF) on F^2	1.044	1.036	1.117
Observed R, wR^2	0.0262, 0.066	0.031, 0.067	0.0564, 0.1404
R_{int}	0.020	0.019	0.0362

Table 2
Selected bond lengths (Å) and bond angles (°) for **1**.

Ru–P1	2.3785(5)	Ru–P2	2.3964(4)
Ru–Cl1	2.4369(3)	Ru–Cl2	2.4225(4)
Ru–N1	2.076(1)	Ru–N2	2.045(1)
C6–N1	1.311(2)	C7–N4	1.325(2)
C7–N3	1.357(2)	N1–Ru–N2	78.45(5)
Cl1–Ru–Cl2	91.44(1)	Cl2–Ru–N2	90.87(4)
Cl1–Ru–N1	99.24(4)	P1–Ru–P2	174.37(1)

Table 3
Selected bond lengths (Å) and bond angles (°) for **2**.

Ru1–Cl1	2.3634(5)	Ru1–P1	2.3536(5)
Ru1–N1	2.119(2)	Ru1–N3	2.096(2)
Ru1–O1	1.975(1)	Ru1–O2	2.004(1)
N3–C21	1.310(2)	N1–C7	1.296(2)
N2–C8	1.297(2)	N4–C22	1.287(2)
Cl1–Ru1–N3	172.76(4)	O1–Ru1–O2	177.69(5)
P1–Ru1–N1	175.42(5)	N3–Ru1–O2	87.29(5)
N1–Ru1–O1	90.51(6)	–	–

Table 4
Selected bond lengths [Å] and bond angles [°] for 3.

Ru1–P1	2.386(1)	Ru1–P2	2.407(1)
Ru1–C8	1.981(5)	Ru1–Cl1	2.436(1)
Ru1–N1	2.069(4)	Ru1–O1	2.060(4)
N3–C8	1.326(6)	N1–C7	1.333(6)
N2–C7	1.360(6)	N1–Ru1–C8	76.0(2)
C8–Ru1–O1	80.8(1)	N1–Ru1–O1	155.8(1)
P1–Ru1–P2	178.55(4)	–	–

ods, SHELXS-97 [25] and WinGX [26] were used to solve all three structures. All non-hydrogen atoms were located in the difference density map and refined anisotropically with SHELXL-97 [25]. All hydrogen atoms were included as idealized contributors in the least squares process. Their positions were calculated using a standard riding model with C–$H_{aromatic}$ distances of 0.93 Å and U_{iso} = 1.2 Ueq. The imidazolium N–H bonds of **1** and **2** as well as the toluene solvate C–H bonds of **3** were located in the difference density map, and refined isotropically. All hydrogen atoms of **1** and **2** were included as idealized contributors in the least squares process but for **3**, OLEX 2 was utilized where the hydrogen atoms were treated by a mixture of independent and constrained refinement [27]. One of the phenyl rings of **1**, specifically that attached to P2 (*i.e.* ring carbons C32–C37), was disordered over two sites with near-orthogonal orientations. The two orientations of the phenyl group were assigned to independent parts during structure refinement and the site occupancy factor allowed to freely vary. The final site occupancy factor for the major orientation of the phenyl ring was 0.53617.

3. Results and discussion

3.1. Synthesis and spectral characterization

The equimolar ratio reactions of bzpy and Hbzp with *trans*-[$RuCl_3(PPh_3)_2$] afforded a diamagnetic complex *cis-Cl*, *trans-P*-[$Ru^{II}Cl_2(bzpy)(PPh_3)_2$] (**1**) and a paramagnetic complex *trans*-[$Ru^{III}(bsp)Cl(PPh_3)_2$] (**3**), respectively. In addition, a '2 + 2' paramagnetic ruthenium(III) complex, [$RuCl(bsp)_2(PPh_3)$] (**2**) was attained from the 1:2 M ratio reaction between *trans*-[$RuCl_2(PPh_3)_3$] and Hbsp. The isolated ruthenium(II/III) complexes exhibits its diverse structural features, despite the fact that similarly structured ligand systems were reacted with the same metal precursor. Both **1** and **3** are stabilized by the *trans axial*-[Ru^X-$(PPh_3)_2$] core {X = II (for **1**) and X = III (for **3**)}. In **1**, the bzpy chelator acts as a neutral bidentate chelator through the imino (N1) and pyridyl (N2) nitrogens, whereas in **3** the coordinated bsp chelator acts as a dianionic tridentate chelator through the deprotonated imino carbon (C8) and phenolic oxygen (O1) as well as the neutral imidazolium nitrogen (N1).

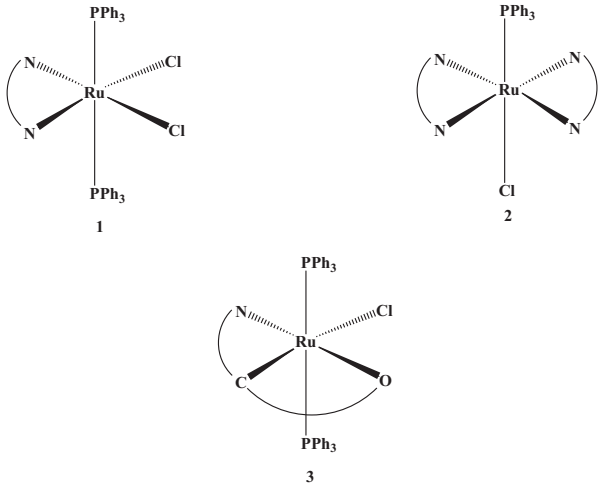

It is commonly found that multidentate Schiff base ligands stabilize the *trans*-$[Ru^{II}(PPh_3)_2]^{2+}$ core through their chelation and diverse donor capabilities. For example, the metal carbonyl complex *trans*-[RuH(cops)CO(PPh_3)$_2$] {Hcops = 2-chlorophenylsalicylaldimine}, where the cops Schiff base moiety acts as a monoanionic bidentate chelator, affords a stable 6-membered chelate ring through the deprotonated phenolic oxygen and imino nitrogen [28]. This is further exemplified, within the bicyclometalled complex, *trans*-[Ru(mbo)CO(PPh_3)$_2$] {H_2mbo = 2-mercaptophenylimino-4-bromophenol}, in which the mbo Schiff base chelates the metal centre *via* the SNO donor set thereby forming 5- as well as 6-membered chelate rings [29]. In another study, efforts to isolated a ruthenium complex with the potentially tetradentate *bis*-Schiff base ligand H_2pmb, {1,2-*bis*(2′-pyridylmethyleneimino)benzene}, the ligand transformed when reacted with *trans*-[$RuCl_2(PPh_3)_3$] to afford the dicationic complex cation *trans*-[$Ru(PPh_3)_2(pbz)_2$]$(ClO)_2$ {pbz = 2-pyridylbenzimidazole} [30].

All the metal complexes (**1**, **2** and **3**) exhibit good solubility in most polar aprotic solvents but partial solubility in alcoholic media. The low molar conductivities of the respective complexes are typical of charge neutrality for ruthenium(II/III) complexes [31]. The ^{1}H NMR spectrum of **1** is dominated by the intense signals of the triphenylphosphine co-ligands which appear as two separate multiplets (at 7.43–7.38 ppm and 7.27–7.22 ppm) (see Fig. S1). More up-field, the aromatic signals of the pyridyl and benzimidazole moieties resonate as less intense multiplets [7.66–7.60 ppm and 7.58–7.54 ppm] respectively. Shifts in both the imino [*H3* at 8.97 ppm] and imidazolium [*H10* at 8.47 ppm] protons of **1** relative to the corresponding signals found within the free-ligand's ^{1}H NMR spectrum (Schiff base and imidazolium protons found at 12.42 and 8.40 ppm, respectively) affirms coordination of the bzpy chelator. Only one signal at 25.57 ppm is found for the two triphenylphosphine co-ligands which indicate that these co-ligands are in similar chemical environments (see Fig. S2).

Within the IR spectra, the single Ru–P bond of 2 [693 cm^{-1}] shows a strong vibrational mode at nearly the same frequency as the *trans*-[$Ru(PPh_3)_2$] unit in **1** [693 cm^{-1}] and **2** [692 cm^{-1}] (see Figs. S3–S5). IR spectral analysis also confirmed coordination through the shifting of the C=N bands of the free–ligands in comparison to the corresponding bands found within the spectra of their complexes. For **1**, the C=N bands of heterocyclic [1635 cm^{-1}] and Schiff base [1606 cm^{-1}] moieties appear at higher frequency compared to the same bands found in the free ligand's [bzpy] IR spectrum [1613 and 1587 cm^{-1}]. Similarly for **3**, the C=N [1679 and 1589 cm^{-1}] bands are more red-shifted with respect to the bands of the free-ligand [1605 and 1589 cm^{-1}]. In contrast for **2**, the C=N [1588 and 1531 cm^{-1}] stretching modes appear at low frequencies in comparison to analogous C=N stretches within in the Hbsp spectrum [1679 and 1573 cm^{-1}]. Weak intensity bands are found both in the IR spectra of **1** [3051 cm^{-1}] and **2** [3062 cm^{-1}] which are attributed to ν(N–H).

Although a soft-ionization technique was employed, the positive mode mass spectrum of **1** showed a peak corresponding to a fragment of the complex minus the chloro co-ligands (see Fig. S6). The peaks of **2** and **3** are detected at 905.049 *m*/*z* [M] and 895.142 *m*/*z* [M–H], respectively. A series of intra-ligand π–π^* transitions [301, 358, 401 and 435 nm] are observed in the UV–Vis spectrum of **1** which were similar to that of the free ligand's electronic transitions (see Fig. S7). A metal-to-ligand-charge transfer transition (MLCT) is observed at 576 nm while no d–d transition was found at longer wavelengths which are as expected for a low spin d^6 octahedral complex [31]. Characteristic of **1**, the highly delocalized chelators afford multiple π–π^* transitions below 400 nm in the UV–Vis spectra of both complexes **2** and **3** (see Fig. S8). Above 400 nm, MLCT [524 (for **2**) and 544 (for **3**) nm] and d–d [705 (for **2**) and 692 (for **3**) nm] transitions are found with significantly lower extinction coefficients.

The paramagnetic centres of complexes **2** and **3** were confirmed by room temperature X-band ESR spectroscopy. The anisotropic solid state ESR spectrum of **2** is nearly identical to the classical rhombic ESR spectra attained for low-spin ruthenium(III) Schiff base complexes, see Fig. 1 [32,33]. The deviation (between 3130 and 3370 G) from the typical rhombic ESR spectrum reflects distortion of the octahedral geometry for **2** [34,35]. The same phenomenon was observed within the poorly resolved solid state ESR spectrum of **3**, where only g_x- and g_y- values were observed, refer to Table 5 and Fig. 2. In the case of the isotropic solution ESR spectra of **2** and **3** in dichloromethane: toluene (1:1), both compounds exhibit broad first derivative features devoid of additional fine structure with centralized g_{iso}-values of 2.113 and 2.110, respectively.

3.2. Electrochemistry

Selected cyclic voltammogram (CV) parameters of the complexes are summarized in Table 6 and their respective CVs are shown in Figs. 3 and 4 and S9. The CVs of **1** and **3** showed one redox couple each whereas the CV of **2** showed two redox couples labeled **A** and **B**, respectively. For **2**, the peak potentials on the squarewave voltammogram (SWV, see Fig. 5) are as expected equal to the calculated halfwave potentials. All the redox couples are quasi-reversible since their peak to peak separations (ΔE) are different than ferrocene (ΔE = 90 mV at 100 mV/s). In addition, all the redox couples showed diffusion controlled behavior with increasing scan rates. For example, see Fig. S10 for the overlay CVs of complex **3** for scan rates ranging from 50 to 200 mV/s, at increments of 25 mV/s. Peak current ratios approaching one, were observed for all complexes which imply the redox couples are for one electron redox processes.

The quasi-reversible redox processes of **1** and **3** were ascribed to the Ru(II/III) redox couples since they have similar halfwave potentials ($E_{½}$) found for other ruthenium(II/III) complexes within literature. Like in the case of the ruthenium(II) complexes, *trans*-[$Ru(H^Rbmp)(PPh_3)_2(CO)(Cl)$], 2-benzylimino-methyl)-4-*R*-phenol (H^Rbmp) in DCM (*vs* Ag|AgCl) with halfwave potentials ranging from 0.62 V to 1.16 V [36]. Similarly, the paramagnetic *trans*-[$Ru^{III}Cl(L)(PPh_3)_2$] {Schiff base (H_2L) ligands derived from benzaldehyde and various functionalized acetic hydrazides} complexes exhibited comparable Ru(II/III) redox couples, under similar experimental conditions [37].

The two redox processes (**A** and **B**) of **2** were both assigned to be metal based redox processes as the CV of the free-ligand (*i.e.* Hbsp)

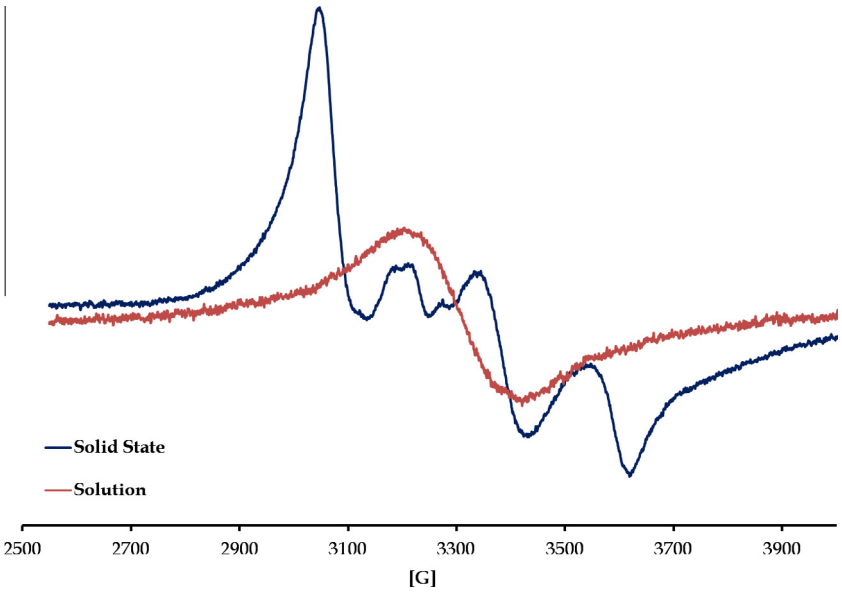

Fig. 1. Solid state and Solution X-band ESR spectra of **2** at 298 K. Instrument settings: microwave bridge frequency, 9.8 GHz; microwave bridge attenuator, 20 dB; modulation frequency, 100 kHz; modulation amplitude, 5 G; centre field, 3500 G.

Table 5
G-values of the respective complexes in the solid state (**A**) and in solution (**B**).

Spectrum	g_x	g_y	g_z	g_{iso}
2-A	2.198	2.090	1.910	–
2-B	–	–	–	2.113
3-A	2.309	2.018	–	–
3-B	–	–	–	2.110

Not observed.

indicated that the compound was not redox active within the same potential window as **A** and **B**, respectively. These redox couples were assigned to the Ru(II/III) [for **A**] and Ru(III/IV) [for **B**] couples, consistent with analogous electrochemical behavior as the ruthenium(III) bipyridine (bpy) complexes, $[Ru(bpy)Cl_3(X)]$ {X = MeOH, PPh_3, 4,4′-bipyridine or CH_3CN} [38]. It has been noted, that the literature range of the halfwave potential differences ($\Delta E_{½}$) for mononuclear ruthenium complexes is 1.2–1.7 V. Within this study, a $\Delta E_{½}$ of 1.358 V for complex **2** was attained which supports the assignments of the respective couples.

The redox couples of the respective complexes were further investigated with spectroelectrochemistry to corroborate the voltammetric assignments. The overlay UV–Vis spectra of **1** showed a distinctive isosbestic point at 603 nm which is due to the appearance of a shoulder (at 681 nm) ascribed to a *d*–*d* electronic transition (see Fig. 6). Occurrence of this metal-based electronic transition implies that the d^6–d^5 system conversion transpired, confirming the Ru(II/III) redox couple in the CV assignment [39]. A characteristic feature is the accompanying decrease in the MLCT (at 576 nm) and becomes progressively red-shifted until 585 nm [40,41].

Applying a controlled negative overpotential (at −0.55 V) for **2** while investigating the redox couple A, the reduction of the paramagnetic ruthenium(III) centre is confirmed by the disappearance of the *d*–*d* transition (at 705 nm) and the formation of a new MLCT

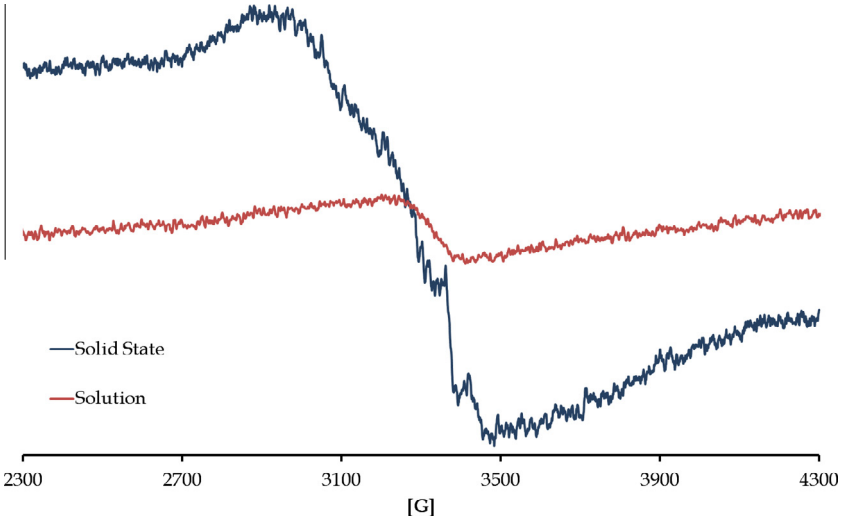

Fig. 2. Solid state and Solution X-band ESR spectra of **3** at 298 K. Instrument settings: microwave bridge frequency, 9.8 GHz; microwave bridge attenuator, 20 dB; modulation frequency, 100 kHz; modulation amplitude, 5 G; centre field, 3500 G.

Table 6
Selected CV parameters (at 100 mV/s) for the complexes **1**, **2** and **3**.

Complex	**1**	**2**		**3**
		A	**B**	
E_{pa} (V)	0.896	−0.433	0.965	0.660
E_{pc} (V)	0.820	−0.497	0.899	0.739
$E_{½}$ (mV)	0.858	−0.465	0.932	0.700
ΔE (mV)	76	64	66	79

band at 574 nm between the two defined isosbestic points (at 447 and 649 nm), see Fig. 7. Another study of a ruthenium(III) complex, [Ru(H_2bpyp)(acac)] {H_2bpyp = 1,2-benzyl-*bis*-(2-(*pyrazol*-4-*yl*)phenol)}, with similar CV traces as **2** showed that the reduction to the Ru(II) species also resulted in the formation of a new MLCT [42].

Nearly quantitative conversion back to **2** occurred when a zero potential was applied, leading to the regeneration of the *d*–*d* transition. At incrementing applied positive potentials, the characteristic feature of the redox couple A, is the intense π–π^* transitions at 259 and 286 nm while a decrease in the rest of the bands were noted, which could imply that ligand-induced oxidation of the metal centre took place (see Fig. 8) [43,44]. These spectroelectrochemical observations of **2** confirm the CV and SWV assignments for redox couples **A** and **B**. Unfortunately for **3**, upon applying potentials between 0.865 and 0.90 V, only diffuse isosbestic points were observed which is typical of the presence of two species within the solution.

3.3. Crystallographic studies

Complexes **1** and **3**·C_7H_8 crystallize in the space group $P\bar{1}$, with two molecules of each occupying the respective triclinic unit cells (*i.e.* Z = 2) whereas four crystallographically identical molecules of **2** (*i.e.* Z = 4) are found within its monoclinic unit cell (see Figs. S10–S12). Similar crystal packing arrangements were attained for complexes **1** and **3**.C_7H_8: two mutual classical hydrogen bonds [N2–H2···N3 = 2.11294 Å] in **1** occur between two respective molecules resulting in a series of molecules aligned parallel with the [*c*]-axis; stabilization of the crystal lattice of **3** is rendered through non-classical hydrogen-bonding which allows the molecules to

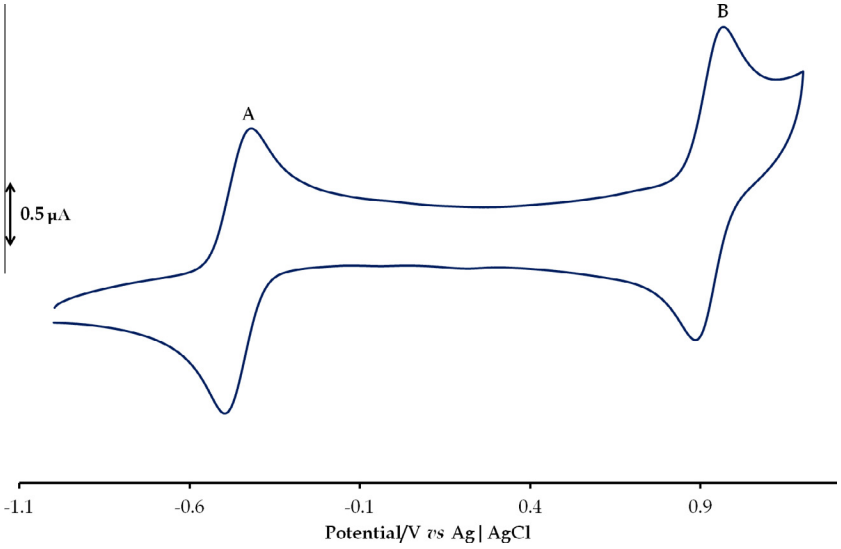

Fig. 3. CV of complex **2** at 100 mV/s between the potential range of −1.0 and +1.2 V.

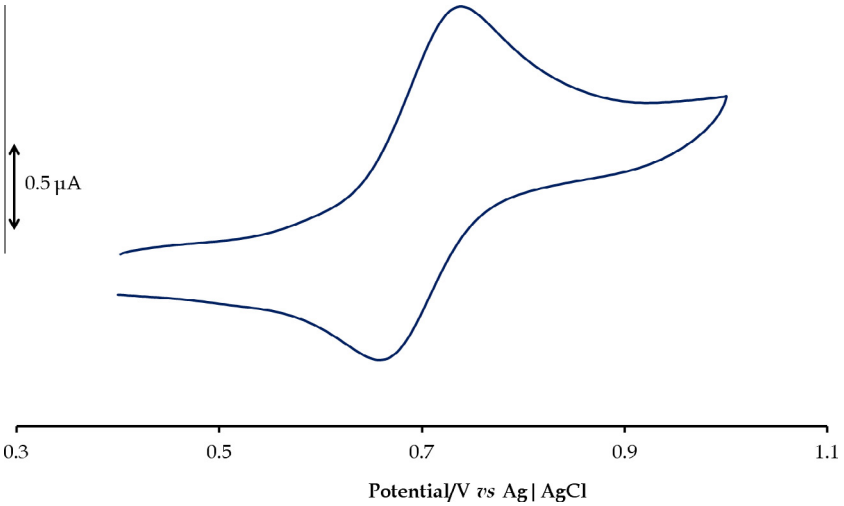

Fig. 4. CV of complex **3** at 100 mV/s between the potential range of −0.4 and +1.0 V.

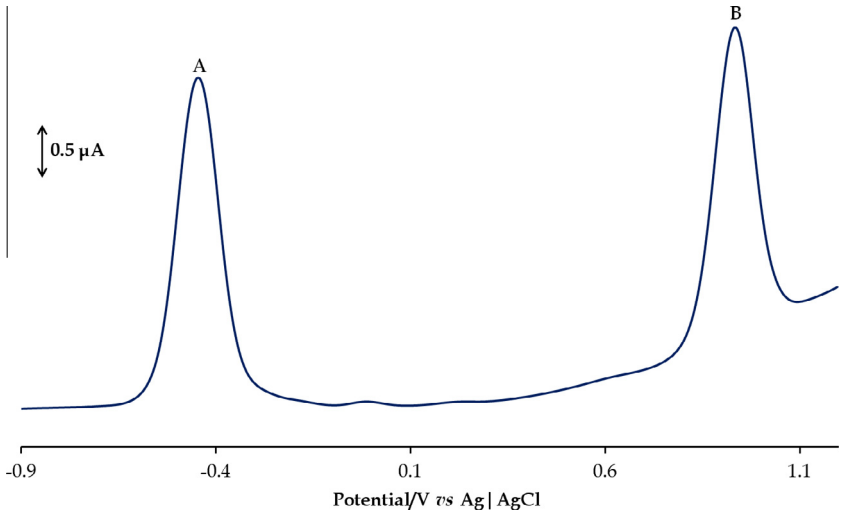

Fig. 5. SWV of complex **2** at 100 mV/s between the potential range of −0.9 and +1.2 V.

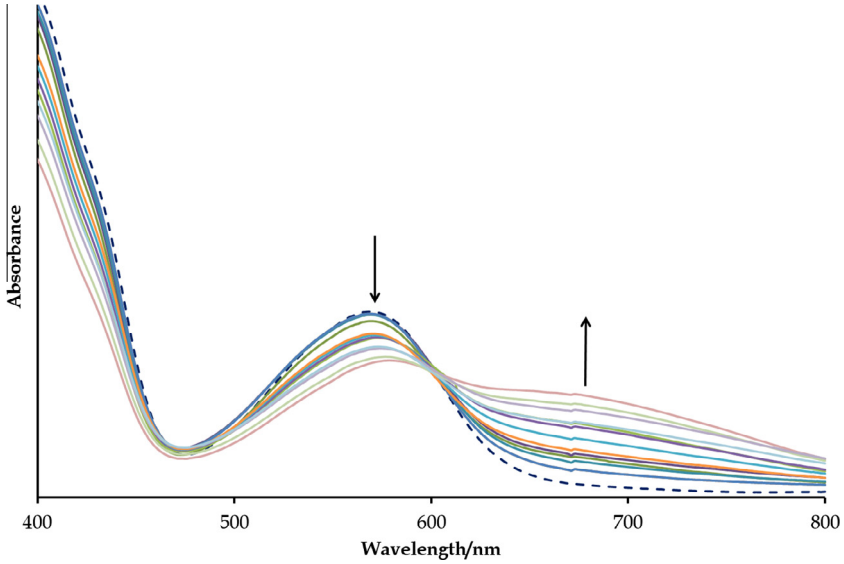

Fig. 6. UV–Vis spectral changes observed for reduction of complex **1** at an applied potential of −0.90 V. The initial spectrum is shown as a dashed blue line. (Colour online.)

stack in columns along the [*c*]-axis. The molecules of **2** run parallel with the [*a*]-axis due to a series of intermolecular interactions [3.87 Å] between the S1-benzothiazole moieties of adjacent molecules.

The effects of cyclometallation are clearly evident from the distortion of the equatorial bond angles compared to the ideal octahedral values. For **1**, the constrained N1–Ru–N2 [78.45(5)°] bite angle forces the Cl1–Ru–Cl2 [91.44(1)°], Cl2–Ru–N2 [90.87(4)°] and [Cl1–Ru–N1 = 99.24(4)°] bond angles wider than the idealized 90° (see Fig. 9). Similarly, the bicyclometalled complex **3** with its two 5-membered chelate rings [bite angles: N1–Ru1–C8 = 76.0(2)° and C8–Ru1–O1 = 80.8(1)°] force the bond angles Cl–Ru1–C8 = 176.4(1)° and N1–Ru1–O1 = 155.8(1)° to deviate from linearity (see Fig. 10). The same phenomenon was observed with complex **2**'s equatorial bond [Cl1–Ru1–N3 = 172.76(4)° and O1–Ru1–O2 = 177.69(5)°] angles which were all less than 180° as ascribed to the 6-membered chelate rings [N3–Ru1–O2 = 87.29(5)° and N1–Ru1–O1 = 90.51(6)°] (see Fig. 11).

In fact, the latter bond angles induces a P1–Ru–N1 [175.42(5)°] axial bond angle which deviates from linearity. For **1**, non-linearity of its axial bond angle [P1–Ru–P2 = 174.37(1)°] is accounted to the interactions between selected phenyl rings of the PPh_3 co-ligands and the imidazolium/pyridyl moieties of the bzpy chelator, see Fig. S14 {**I** = 3.748 Å, **II** = 3.553 Å and **III** = 3.575 Å}. Consequently, the respective non-coordinating heterocyclic moieties are found out of plane with the pyridyl (of **1**) and deprotonated phenolic (of **2**) rings. More specifically, the pyridyl moiety is slightly out of plane (by 11.07°) with respect to the benzimidazole moiety. Furthermore, the benzothiazole moieties are at different angles [54.72° with respect to the S1-benzothiazole and 11.53° with respect to the S2-benzothiazole] out of the plane of the deprotonated phenolic rings which are due to the combined effects of the inter- and intramolecular steric interactions. Unlike **1** and **2**, no co-planar phenyl rings of the PPh_3 co-ligands were found with respect to the bzp chelator of **3** which lead to a straighter backbone [P1–Ru1–P2 = 178.55(4)°]. The axial linearity of **3** is also clearly evident from the Ru–P [Ru1–P1 = 2.386(1) Å and Ru1–P2 = 2.407(1) Å] bond distance being nearly equal.

The *cis*–chloro coordination bonds of **1** [Ru-Cl1 = 2.4369(3) Å and Ru–Cl2 = 2.4225(4) Å] are nearly equidistant which implies that the *trans*-influence on the N1 and N2 nitrogen atoms are approximately similar. The other coordination bonds of Ru–N1

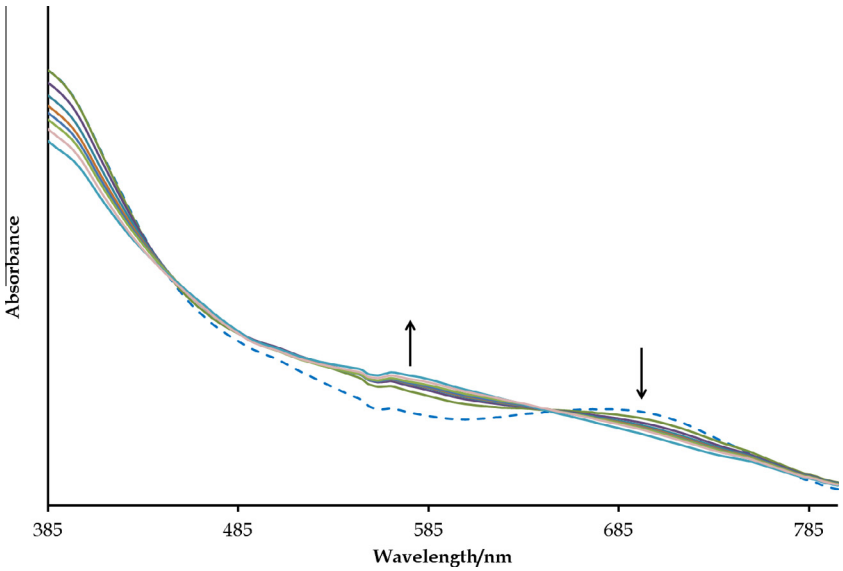

Fig. 7. UV–Vis spectral changes observed for reduction of complex **2** at potentials of redox couple **B**, at an applied potential −0.55 V. The initial spectrum is shown as a dashed blue line. (Colour online.)

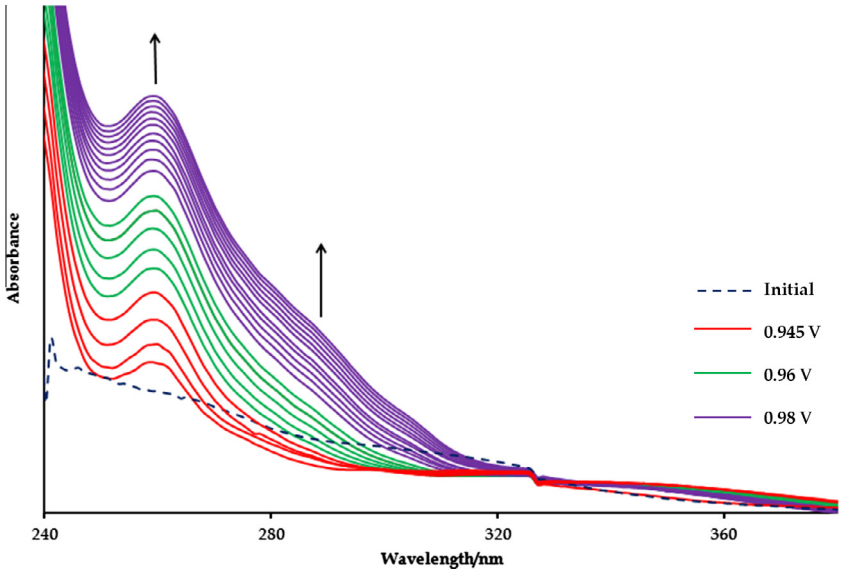

Fig. 8. UV–Vis spectral changes observed for reduction of complex **2** at potentials of redox couple **B**, at incrementing applied potentials. The initial spectrum is shown as a dashed blue line. (Colour online.)

[2.076(1) Å] and Ru–N2 [2.045(1) Å] are typical of a ruthenium(II) metal centre bonded to a pyridyl or Schiff base nitrogens, respectively. For example, the organoruthenium(II) complex, *trans-Cl*, *cis-CO*-[Ru(CO)$_2$(spy)Cl$_2$] {spy = *N*-((pyridine-2-*yl*)methylene)-thiazole} has similar Ru–N$_{\text{Schiff base}}$ and Ru–N$_{\text{pyridyl}}$ bond lengths of 2.169(4) and 2.091(5) Å [45]. Comparatively, the stronger Lewis acidic character of the paramagnetic ruthenium(III) centres compared to the diamagnetic metal centre of **1**, afforded selected shorter analogous coordination sphere bonds for **2** [Ru1–P1 = 2.3536(5) Å, Ru1–N1 = 2.119(2) Å and Ru–N3 = 2.096(2) Å] and **3** [Ru–P1 = 2.3785(5) Å, Ru–P2 = 2.3964(4) Å and Ru1–N1 = 2.069(4) Å]. However, the metal to chloride bond distances for **2** [2.3634(5) Å] and **3** [2.436(1) Å] were different, which is largely accounted to the difference in *trans*-influence experience by the various chloride ions. In addition, similar deprotonated phenolic oxygens to ruthenium(III) bond lengths were found for **2** [Ru1–O2 = 2.004(1) Å] and **3** [Ru1–O1 = 1.975(1) and Ru1–O2 = 2.004(2) Å], respectively. The difference in the imino coordination bonds are ascribed to the varied *trans*-influence on the imino nitrogens.

The rare metal carbene [Ru1–C8 = 1.981(5) Å] bond distance were shorter than the analogous bond [Ru–C$_{\text{Schiff base}}$ = 2.048(7) Å] found in the ruthenium(II) complex, *trans*-[Ru(cmp)(CO)Cl(PPh$_3$)$_2$] {cmp = methyl-4-((5-chloropyridin-2-*yl*-imino)methyl)benzoate} which as expected due to the lower oxidation state of the latter [46]. Nitrogen heterocyclic carbene (NHC) ruthenium complexes have been widely researched due to their optimal catalytic properties, like in hydroformylation, olefin methasis as well as hydrogen-transfer reactions [40,41]. More recently, the first ruthenium chemotherapeutic drug, NAMI-A, *trans*-[RuCl$_4$(DMSO)(Im)](ImH) {Im = imidazole} has recently entered Phase II clinical trials due to its optimal antimetastatic cancer activity which is accompanied

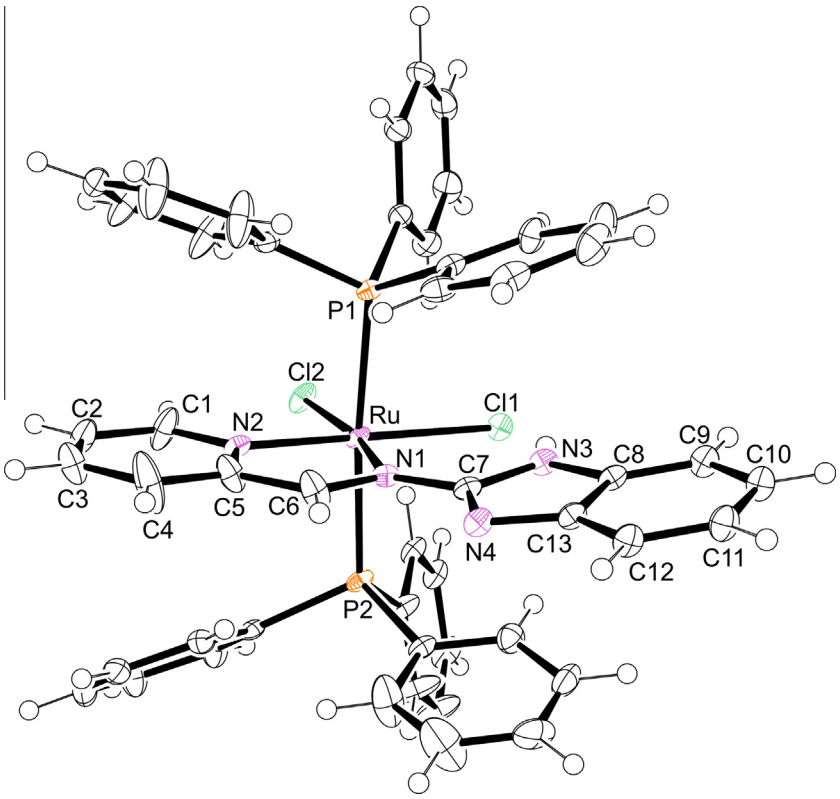

Fig. 9. An ORTEP view of complex **1** showing 50% probability displacement ellipsoids and the atom labeling.

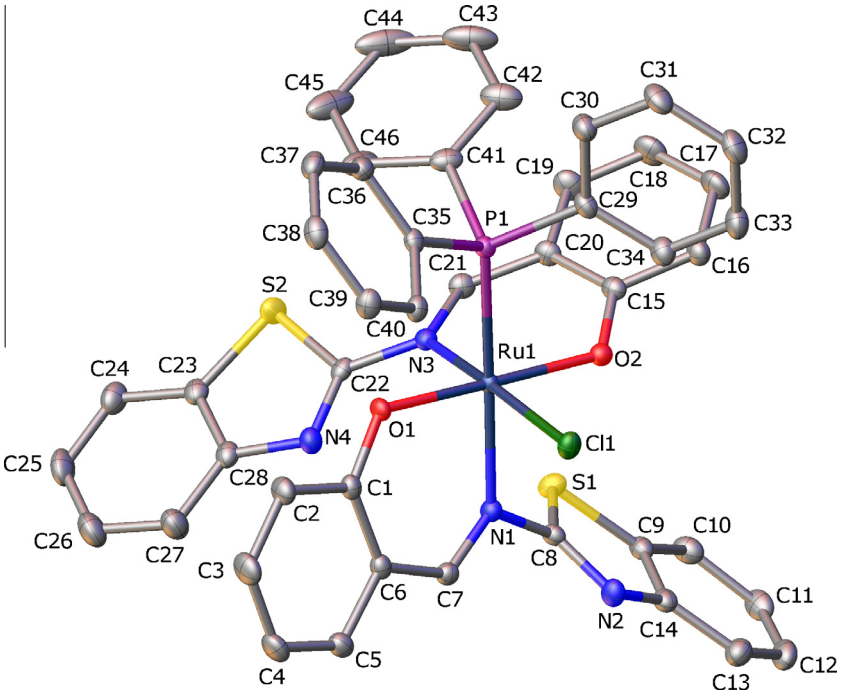

Fig. 10. An ORTEP view of complex **2** showing 50% probability displacement ellipsoids and the atom labeling. Hydrogen atoms have been omitted due to clarity.

with fewer significant side effects than platinum-based metallo-pharmaceuticals [47]. This has led to an interest of exploring the biological activities of NHC ruthenium complexes, *e.g.*, the NHC ruthenium(II) complexes, *cis*-[Ru(η^6-cymene)Cl_2(2R-bz)] {where R can be methyl, ethyl, isopropanol or benzyl subsitituents on the nitrogen atoms of the bz moiety} have shown to exhibit various biological activities ranging from DNA intercalation to protease inhibitor capabilities [48].

Similar bond lengths were attained for the individual {C=N}$_{Schiff\ base}$ [C6–N1 = 1.311(2) Å (for **1**) and C8–N3 = 1.327(6) Å] (for **3**)] and

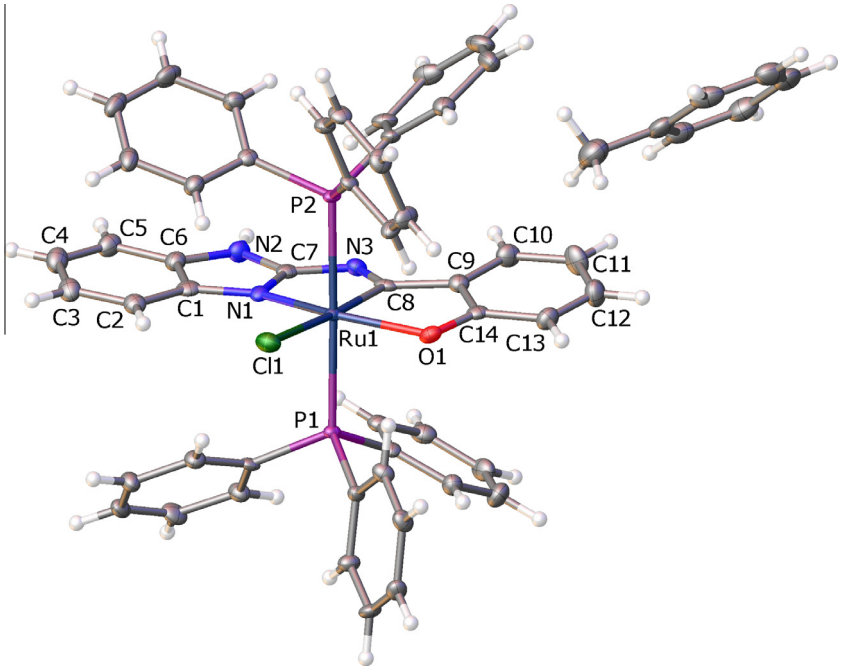

Fig. 11. An ORTEP view of complex **3**·C_7H_8 showing 50 % probability displacement ellipsoids and the atom labeling.

{C═N}$_{Heterocyclic}$ [C7–N4 = 1.325(2) Å (for **1**) and C7–N1 = 1.333(6) Å (for **3**)] bond distances as the nitrogen atoms are sp^2 hydridized nitrogens; but the aforementioned C═N bonds were still shorter than the carbon to sp^3 hybridized nitrogen bonds within their individual heterocyclic moieties [C7–N3 = 1.357(2) Å (for **1**) and N2–C7 = 1.360(6) Å (for **3**)]. Within the bsp chelators (of **2**), the imino bond [N3–C21 = 1.310(2) Å and N1–C7 = 1.296(2) Å] distances were typical for ruthenium(III) complexes with Schiff base chelates; [49] while the C═N bond [C8–N2 = 1.297(2) Å and C22–N4 = 1.287(2) Å] (within the benzothiazole rings) lengths were shorter despite having the same bond order but were comparable for transition metal complexes with non coordinating benzothiazole moieties [50,51].

4. Conclusion

Novel ruthenium complexes with Schiff base chelates containing heterocyclic moieties were isolated. Despite the structural similarities of the ligands, ruthenium(II/III) complexes with unique structural features were isolated. Structural elucidations of the complexes were confirmed by X-ray crystallography and their redox properties were probed *via* cyclic voltammetry. ESR studies of **2** and **3** confirmed the rhombic nature of the respective complexes.

Acknowledgements

We are grateful to the University of KwaZulu-Natal and the National Research Foundation of South Africa for financial support.

Appendix A. Supplementary data

CCDC 963372, 963373 and 963374 contains the supplementary crystallographic data for **1**, **2** and **3**·C_7H_8. These data can be obtained free of charge via http://www.ccdc.cam.ac.uk/conts/retrieving.html, or from the Cambridge Crystallographic Data Centre, 12 Union Road, Cambridge CB2 1EZ, UK; fax: (+44) 1223-336-033; or e-mail: deposit@ccdc.cam.ac.uk. Supplementary data associated with this article can be found, in the online version, at http://dx.doi.org/10.1016/j.poly.2014.02.009.

References

[1] M. Groessl, E. Reisner, C.G. Hartinger, R. Eichinger, O. Semenova, A.R. Timerbaev, M.A. Jakupec, V.B. Arion, B.K. Keppler, J. Med. Chem. 50 (2007) 2185.
[2] M.A. Sgambellone, A. David, R.N. Garner, K.R. Dunbar, C. Turro, J. Am. Chem. Soc. 135 (2013) 11274.
[3] C. Ming Che, F. Siu, Curr. Opin. Chem. Biol. 14 (2010) 255.
[4] M.J. Clarke, Coord. Chem. Rev. 232 (2002) 69.
[5] P. Heffeter, B. Atil, K. Kryeziu, D. Groza, G. Koellensperger, W. Körner, U. Jungwirth, T. Mohr, B.K. Keppler, W. Berger, Eur. J. Cancer, 2013. Available from: <http://dx.doi.org/10.1016/j.ejca.2013.05.018>.
[6] M. Ravera, E. Gabano, S. Baracco, M. Sardi, D. Osella, Inorg. Chim. Acta 361 (2008) 2879.
[7] S. Kapitza, M.A. Jakupec, M. Uhl, B.K. Keppler, Brigitte Marian, Cancer Lett. 226 (2005) 115.
[8] M.P. Chelopo, S.A. Pawar, M.K. Sokhela, T. Govender, H.G. Kruger, G.E.M. Maguire, Eur. J. Med. Chem. 66 (2013) 407.
[9] Y. Chen, M. Qin, L. Wang, H. Chao, L. Ji, A. Xu, Biochimie, 2013. Available from: <http://dx.doi.org/10.1016/j.biochi.2013.07.016>.
[10] S. David, R.S. Perkins, F.R. Fronczek, S. Kasiri, S.S. Mandal, R.S. Srivastava, J. Inorg. Biochem. 111 (2012) 33.
[11] F. Dosio, B. Stella, A. Ferrero, C. Garino, D. Zonari, S. Arpicco, L. Cattel, S. Giordano, R. Gobetto, Int. J. Pharm. 440 (2013) 221.
[12] F.R. Pavan, G.V. Poelhsitz, M.I.F. Barbosa, S.R.A. Leite, A.A. Batista, J. Ellena, L.S. Sato, S.G. Franzblau, V. Moreno, D. Gambino, C.Q.F. Leite, Eur. J. Med. Chem. 46 (2011) 5099.
[13] J. De Pasquale, N.J. White, E.J. Ennis, M. Zeller, J.P. Foley, E.T. Papish, Polyhedron 58 (2013) 162.
[14] A. Grigoratos, N. Katsaros, Inorg. Chim. Acta 108 (1985) 41.
[15] S.O. Pinheiro, J.R. de Sousa, M.O. Santiago, I.M.M. Carvalho, A.L.R. Silva, A.A. Batista, E.E. Castellano, J. Ellena, Í.S. Moreira, I.C.N. Diógenes, Inorg. Chim. Acta 359 (2006) 391.
[16] F.E. Fernández, M. Puerta, P. Valerga, Inorg. Chem 25 (2013) 6502.
[17] J.G. Małecki, A. Maron, Polyhedron 40 (2012) 125.
[18] H. Sharma, H.J. Guadalupe, J. Narayanan, H. Hofeld, T. Pandiyan, N. Singh, Anal. Methods 5 (2013) 3880.
[19] L. Oehninger, M. Stefanopoulou, H. Alborzinia, J. Schur, S. Ludewig, K. Namikawa, A. Muñoz-Castro, R.W. Köster, K. Baumann, S. Wölfl, W.S. Sheldrick, Dalton Trans. 42 (2013) 1657.
[20] A. Singh, B. Chetia, S.M. Mobi, G. Das, P.K. Iyer, B. Mondal, Polyhedron 27 (2008) 1983.
[21] G.G. Mohamed, Z.H. Abd El-Wahab, J. Therm. Anal. Calorim. 73 (2003) 347.
[22] Z.M. Zaki, Spec. Lett. 31 (1998) 757.

[23] R.H. Blessing, Acta Crystallogr., Sect. A 51 (1995) 33.
[24] Bruker APEX2, SAINT and SADABS,. Bruker AXS Inc., Madison, Wisconsin, USA, 2010.
[25] G.M. Sheldrick, Acta Crystallogr., Sect. A 64 (2008) 112.
[26] L.J. Farrugia, J. Appl. Crystallogr. 45 (2012) 849.
[27] O.V. Dolomanov, L.J. Bourhis, R.J. Gildea, J.A.K. Howard, H. Puschmann, J. Appl. Crystallogr. 42 (2009) 339.
[28] J.D.E.T. Wilton-Ely, M. Wang, S.J. Honarkhah, D.A. Tocher, Inorg. Chim. Acta 358 (2005) 3218.
[29] M.M. Tamizh, K. Mereiter, K. Kirchner, R. Karvembu, J. Organomet. Chem. 700 (2012) 194.
[30] D. Mishra, S. Naskar, R.J. Butcher, S.K. Chattopadhyay, Inorg. Chim. Acta 358 (2005) 3115.
[31] N.G. Tsierkezos, A.I. Philippopoulos, Inorg. Chim. Acta 362 (2009) 3079.
[32] A.K. Das, R. Hübner, B. Sarkar, J. Fiedler, S. Záliš, G.K. Lahiric, W. Kaim, Dalton Trans. 41 (2012) 8913.
[33] K. Nagaraju, S. Pal, J. Organomet. Chem. 737 (2013) 7.
[34] C.P. Matos, A. Valente, F. Marques, P. Adão, M.P. Robalo, R.F.M. de Almeida, J.C. Pessoa, I. Santos, M.H. Garcia, A.I. Tomaz, Inorg. Chim. Acta 394 (2013) 616.
[35] K. Nagaraju, R. Raveendran, S. Pal, S. Pal, Polyhedron 33 (2012) 52.
[36] R. Raveendran, S. Pal, J. Organomet. Chem. 695 (2010) 630.
[37] R. Raveendran, S. Pal, J. Organomet. Chem. 692 (2007) 824.
[38] E. Eskelinen, P. Da Costa, M. Haukka, J. Electroanal. Chem. 579 (2005) 257.
[39] T. Hamaguchi, Y. Kurashige, I. Ando, Inorg. Chim. Acta 405 (2013) 410.
[40] V.R. de Souza, G.S. Nunes, R.C. Rocha, H.E. Toma, Inorg. Chim. Acta 348 (2003) 50.
[41] R.M. Berger, Inorg. Chem. 29 (1990) 1920.
[42] G.F. Frey, Z.R. Bell, J.C. Jeffery, M.D. Ward, Polyhedron 20 (2001) 3231.
[43] R. Jana, B. Schwederski, J. Fiedler, W. Kaim, Polyhedron 44 (2012) 174.
[44] L. Giovagnini, S. Sitran, I. Castagliuolo, P. Brun, M. Corsini, P. Zanello, A. Zoleo, A. Maniero, B. Biondi, D. Fregona, Dalton Trans. (2008) 6699.
[45] S. Kundu, D. Sarkar, M.S. Jana, A.K. Pramanik, S. Jana, T.K. Mondal, J. Mol. Struct. 1035 (2013) 277.
[46] S. Mandal, D.K. Seth, P. Gupta, Inorg. Chim. Acta 397 (2013) 10.
[47] M.J. Clarke, Coord. Chem. Rev. 236 (2003) 209.
[48] L. Oehninger, M. Stefanopoulou, H. Alborzinia, J. Schur, S. Ludewig, K. Namikawa, A. Muñoz-Castro, R.W. Köster, K. Baumann, S. Wölfl, W.S. Sheldrick, I. Otta, Dalton Trans. 42 (2013) 1657.
[49] R. Raveendran, S. Pal, Polyhedron 27 (2008) 655.
[50] K.C. Potgieter, T.I.A. Gerber, E. Hosten, Chem. Commun. 24 (2012) 231.
[51] H. Yu, X. Fang, K. Zhang, M. Lin, D. Gao, M. Huanga, J. Wanga, Cryst. Eng. Commun. 15 (2013) 343.